



Combining Poisson singular integral and total variation prior models in image restoration [☆]

Pablo Ruiz ^a, Hiram Madero-Orozco ^b, Javier Mateos ^{a,*},
Osslan Osiris Vergara-Villegas ^c, Rafael Molina ^a, Aggelos K. Katsaggelos ^d

^a Departamento de Ciencias de la Computación e I.A., Universidad de Granada, Spain

^b Departamento de Ingeniería Eléctrica y Computación, Universidad Autónoma de Ciudad Juárez, Chihuahua, Mexico

^c Departamento de Ingeniería Industrial y Manufactura, Universidad Autónoma de Ciudad Juárez, Chihuahua, Mexico

^d Electrical Engineering and Computer Science Department, Northwestern University, Evanston, IL, USA

ARTICLE INFO

Article history:

Received 4 June 2013

Received in revised form

16 September 2013

Accepted 23 September 2013

Available online 14 October 2013

Keywords:

Deblurring

Denoising

Bayesian image restoration

Total Variation

Poisson Singular Integral

ABSTRACT

In this paper, a novel Bayesian image restoration method based on a combination of priors is presented. It is well known that the Total Variation (TV) image prior preserves edge structures while imposing smoothness on the solutions. However, it tends to oversmooth textured areas. To alleviate this problem we propose to combine the TV and the Poisson Singular Integral (PSI) models, which, as we will show, preserves the image textures. The PSI prior depends on a parameter that controls the shape of the filter. A study on the behavior of the filter as a function of this parameter is presented. Our restoration model utilizes a bound for the TV image model based on the majorization–minimization principle, and performs maximum *a posteriori* Bayesian inference. In order to assess the performance of the proposed approach, in the experimental section we compare it with other restoration methods.

© 2013 Elsevier B.V. All rights reserved.

1. Introduction

In the digital age we live in, millions of pictures are taken every day with digital cameras or mobile devices like cell-phones, tablets, etc. Those pictures are intended to be a detailed representation of reality, but very often the captured image is degraded by blur and noise. Blur can occur, for instance, by movement during the capturing

process or because the scene is out of focus. Furthermore, noise can be introduced, for instance, by sensor imperfections, poor illumination or communication errors [1]. When such problems occur, the usual solution is to take another picture, but sometimes it is not possible to retake the same picture and the moment is lost. Image restoration handles this problem by estimating the original image from its blurred and noisy observation.

The image restoration problem has been addressed successfully using different approaches (see [2] for a detailed review of classical models and [1] for references of recent restoration models). When only noise is present, that is, the image is crisp but noisy, denoising algorithms such as [3–5] can be used (see [6] for a recent review and comparison of denoising method). However, if the image is also blurred, image restoration methods, that handle both blurring and noise, are needed. Many restoration methods utilize a Total Variation (TV) image prior or regularizer [7–10]. TV is well known for preserving object

[☆] This research was supported by CONACYT, by the Spanish Ministry of Economy and Competitiveness under Project TIN2010-15137, the European Regional Development Fund (FEDER), the CEI BioTic at the Universidad de Granada and, in part, by the US Department of Energy Grant DE-NA0000457.

* Corresponding author. Tel.: +34 958240801.

E-mail addresses: mataran@decsai.ugr.es (P. Ruiz),
al116148@alumnos.uacj.mx (H. Madero-Orozco),
jmd@decsai.ugr.es (J. Mateos),
overgara@uacj.mx (O. Osiris Vergara-Villegas),
rms@decsai.ugr.es (R. Molina),
aggk@eecs.northwestern.edu (A.K. Katsaggelos).

boundaries (edges) and removing noise, but it often eliminates image texture, which plays an important role in visual quality.

Different methods have been developed to preserve image textures. Chen et al. [11] adopt a two-step non-iterative processing procedure which first employs a simplified Wiener filter to obtain a distortion free but noisy estimate, and then utilizes a modified non-local means filter to reduce the leaked colored noise in order to obtain a good texture-preserving restoration.

Within the Bayesian paradigm, constraints on the characteristics of the resulting image are formulated as prior distributions. Two of the most classical prior distributions are conditional and simultaneous autoregressive (CAR and SAR) models [12]. They impose smoothness constraints on the original image and are able to preserve image textures better than TV, unfortunately, they over-smooth edge regions.

Carasso proposes in [13] a new approach to preserve image textures. He formulates the image restoration problem in a Lipschitz space where a broader set of images can be accommodated. The central idea is the introduction of the Poisson singular integral (PSI), which recovers the image texture in cases where TV fails. PSI is also utilized in [14], where it is combined with a curvelet-type decomposition to preserve textures while controlling the noise. Other methods based on wavelets and curvelets have also been proposed in combination with shrinkage-threshold rules [1,15] to capture and preserve sharp features in the image.

Wang et al. [16] proposes to combine a weighted anisotropic TV (WATV) [17] and tetrolet shrinkage [18]. WATV can recover sharp and clear edges along four directions, but this approach also eliminates image textures. To alleviate this problem, the tetrolet transform is used in combination with a TV regularizer.

Recently, a new approach that combines different priors has been used to solve super resolution [19], blind deconvolution [20,21], astronomical and natural image [22] restoration problems. The idea behind the combination of priors is that using priors that preserve edges jointly with priors that preserve textures can achieve better reconstructions than simply using one image prior. Notice that this idea is also related to the model in [20].

Using this approach, Vega et al. [22] tackle image restoration in Astronomy by combining a prior based on the ℓ_1 norm of the horizontal and vertical first order differences which preserve edges and a simultaneous autoregression (SAR) prior model which preserves image texture. A similar approach was used by Villena et al. in super resolution problems [19]. The problem of blind deconvolution is addressed in [20] using Bayesian inference with super-Gaussian sparse image priors. This methodology can be used in blind and non-blind image deconvolution problems with the only knowledge of the noise variance.

Based on these recent developments, in this paper we propose a novel Bayesian image restoration algorithm that uses a combination of the TV and PSI prior models in order to preserve different properties on the restored image. This combination takes advantage of each prior: the TV prior preserves edge structure and removes the noise while the PSI prior preserves the image textures.

The rest of the paper is organized as follows. In Section 2, the TV and PSI models are presented within the Bayesian framework, their relations are established and an analysis of the PSI is presented. Section 3 discusses the inference procedure and proposes our algorithm to restore the images. Section 4 contains the experimental results and Section 5 concludes the paper.

2. Bayesian modeling

The Bayesian paradigm is one of the most popular tools in image restoration (see [9] and references therein). The use of prior distributions that impose constraints on the estimates and act as regularizers allows the introduction of additional information in the restoration process. In this section, we first model the image acquisition process to obtain the observed image from the original one and the blur and then introduce the proposed combination of priors models we will use.

2.1. Observation model

It is usual to model the degradation process as a convolution between the original image and a known blurring operator that is expressed in vector–matrix notation as

$$\mathbf{y} = \mathbf{H}\mathbf{x} + \mathbf{n}, \tag{1}$$

where \mathbf{x} and \mathbf{y} are column vectors of size $P = m \times n$ obtained by lexicographically ordering the pixels in the original and observed image, respectively, \mathbf{H} is a known blurring matrix of size $P \times P$, and \mathbf{n} is Gaussian additive white noise with zero mean and precision β . From this degradation model, the conditional probability distribution of the observed image \mathbf{y} given the original image \mathbf{x} and the noise precision parameter, β , is given by

$$p(\mathbf{y}|\mathbf{x}, \beta) \propto \exp\left(-\frac{\beta}{2} \|\mathbf{y} - \mathbf{H}\mathbf{x}\|^2\right). \tag{2}$$

2.2. Image model

Digital images are discrete representations of continuous bidimensional signals, i.e., each image \mathbf{x} is assumed to have been obtained by discretizing a continuous bidimensional signal \mathbf{f} that belongs to the space of signals with bounded p -norm ($L^p(\mathbb{R}^2)$). In this space the continuous Total Variation (TV_c) semi-norm is defined as

$$TV_c(\mathbf{f}) = \int_{\mathbb{R}^2} \|\nabla \mathbf{f}(\mathbf{s})\|^2 ds. \tag{3}$$

Notice that for constant signal $\mathbf{f} \neq 0$, $TV_c(\mathbf{f}) = 0$ and, therefore, TV_c is not a norm. The equivalent semi-norm in discrete case is the Total Variation function, that is defined as

$$TV(\mathbf{x}) = \sum_{i=1}^P \sqrt{\Delta_i^h(\mathbf{x})^2 + \Delta_i^v(\mathbf{x})^2}, \tag{4}$$

where the operators $\Delta_i^h(\mathbf{x})$ and $\Delta_i^v(\mathbf{x})$ correspond to the horizontal and vertical first order differences at pixel i , respectively. In other words, $\Delta_i^h(\mathbf{x}) = x_i - x_{l(i)}$ and

$\Delta_i^v(\mathbf{x}) = x_i - x_{a(i)}$ with $l(i)$ and $a(i)$ denoting the nearest neighbors to the left and above of pixel i , respectively. Using this energy function we obtain the so-called TV [9] prior defined as

$$p_1(\mathbf{x}|\alpha_1) \propto \exp(-\alpha_1 \text{TV}(\mathbf{x})). \quad (5)$$

The TV prior has the advantage of preserving the edge structure while imposing smoothness on the solution.

This model implicitly imposes that the continuous total variation is bounded. However, it is demonstrated in [23] that the continuous signals corresponding to images with high texture have an unbounded total variation, and for this reason, the TV model fails on highly textured images.

Following [13], the space of bounded total variation ($BV(\mathbb{R}^2)$) is composed of all signals $\mathbf{f} \in L^p(\mathbb{R}^2)$ satisfying the constrain

$$\int_{\mathbb{R}^2} \|\mathbf{f}(\mathbf{s}+\mathbf{d}) - \mathbf{f}(\mathbf{s})\| \, d\mathbf{s} \leq \text{Const} \|\mathbf{d}\|. \quad (6)$$

To preserve textures, Carasso [13] proposes to work in the Lipschitz (Besov) space $\Lambda(\alpha, 2, \infty)$, where the weaker

constraint

$$\left\{ \int_{\mathbb{R}^2} \|\mathbf{f}(\mathbf{s}+\mathbf{d}) - \mathbf{f}(\mathbf{s})\|^2 \, d\mathbf{s} \right\}^{1/2} \leq \text{Const} \|\mathbf{d}\|^\alpha, \quad 0 < \alpha < 1 \quad (7)$$

must be satisfied.

In [24] it is shown that \mathbf{f} belongs to the Lipschitz space $\Lambda(\alpha, 2, \infty)$ if, and only if

$$\sup_{t>0} t^{-\alpha} \|\mathbf{U}^t \mathbf{f} - \mathbf{f}\|_2 < \infty, \quad (8)$$

where \mathbf{U}^t is the Poisson integral operator defined as

$$\mathbf{U}^t \mathbf{f} = \int_{\mathbb{R}^2} \phi(x, y, t) \mathbf{f}(x-u, y-v) \, du \, dv, \quad (9)$$

and ϕ is the Poisson kernel in \mathbb{R}^2

$$\phi(x, y, t) = \frac{t}{2\pi(x^2 + y^2 + t^2)^{3/2}}. \quad (10)$$

Carasso [13] shows that this space contains a rich and significant class of images, and proposes a restoration method for them. To force the signal \mathbf{f} to be in $\Lambda(\alpha, 2, \infty)$, in [13] it is imposed that $\int_0^t \|\mathbf{U}^s \mathbf{f} - \mathbf{f}\|_2^2 \, ds$ is bounded, and it

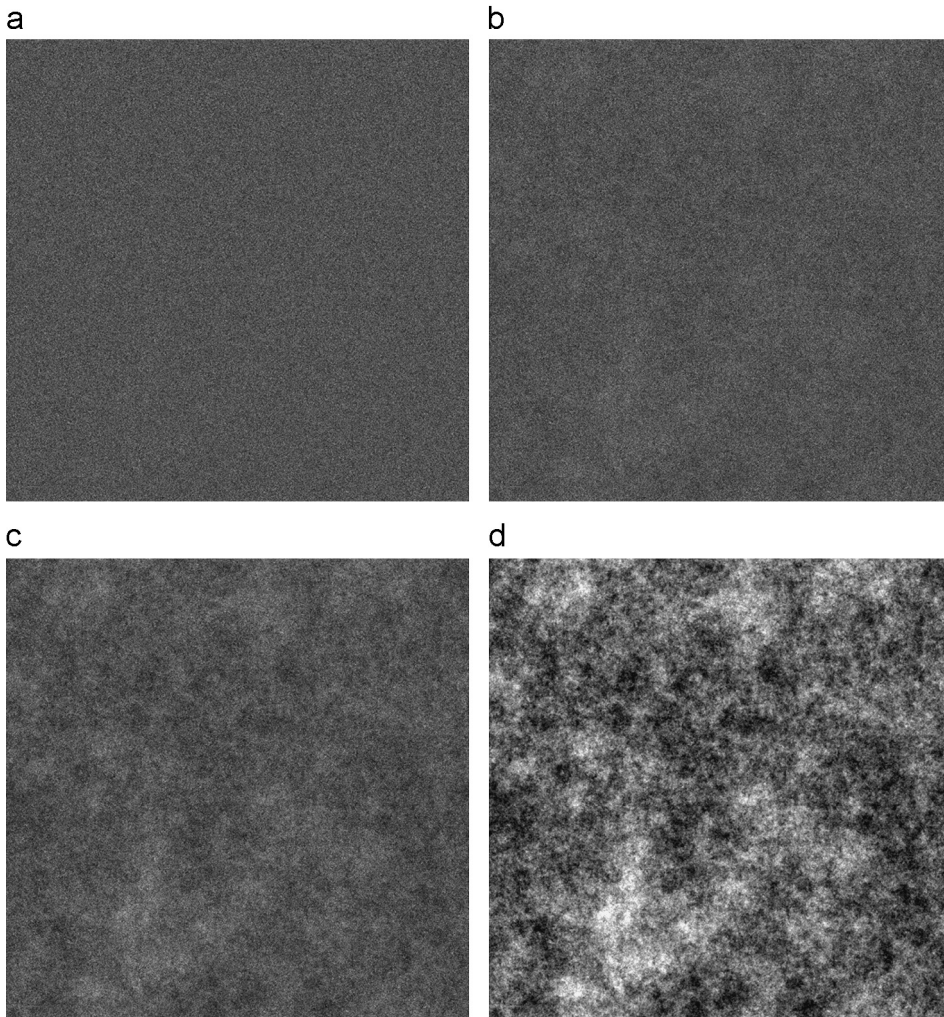


Fig. 1. Realizations of the PSI prior model for different values of t : (a) $t=1$, (b) $t=0.1$, (c) $t=0.03$ and (d) $t=0.001$.

is demonstrated that

$$\int_0^t \|\mathbf{U}^s \mathbf{f} - \mathbf{f}\|^2 ds = \|\mathbf{Z}_c \mathbf{f}\|_2^2, \tag{11}$$

where \mathbf{Z}_c is the continuous convolution operator of the filter \mathbf{z} , which is defined in the Fourier domain as follows:

$$\mathbf{z}(\xi, \nu, t) = \left(t + \frac{4e^{-t\rho} - e^{-2t\rho} - 3}{2\rho} \right)^{1/2}, \tag{12}$$

where ξ, ν are coordinates in the Fourier domain, $\rho = \sqrt{\xi^2 + \nu^2}$. By continuity, we have $\mathbf{z}(0, 0, t) = 0$. The obtained filter is normalized so that its squared components add to 1.

Using the discrete version of the convolution operator of the filter \mathbf{z} , \mathbf{Z} , which is obtained by sampling the filter at the resolution of the image, we can define the PSI based prior model

$$p_2(\mathbf{x}|\alpha_2) \propto \exp\left(-\frac{\alpha_2}{2} \|\mathbf{Z}\mathbf{x}\|^2\right), \tag{13}$$

where α_2 is the prior precision parameter.

The filter \mathbf{z} in Eq. (12) depends on a parameter t . To illustrate the effect of this parameter on the prior, Fig. 1

shows a set of realizations of the PSI prior model in Eq. (13) with precision $\alpha_2 = 1$, for four different values of t . As it can be observed t controls the smoothness of the

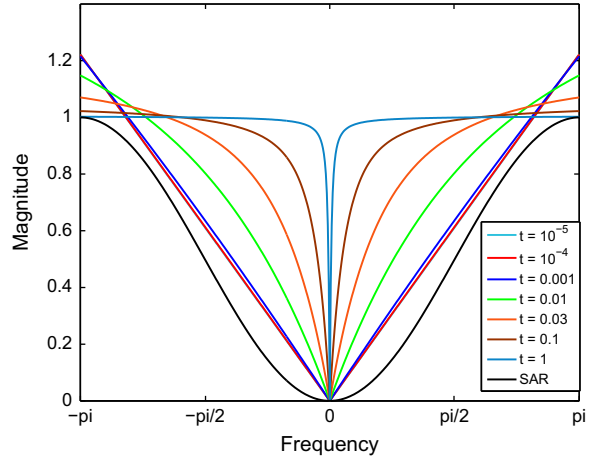


Fig. 3. Transversal cut of SAR and PSI filters in Fourier domain for different values of t .

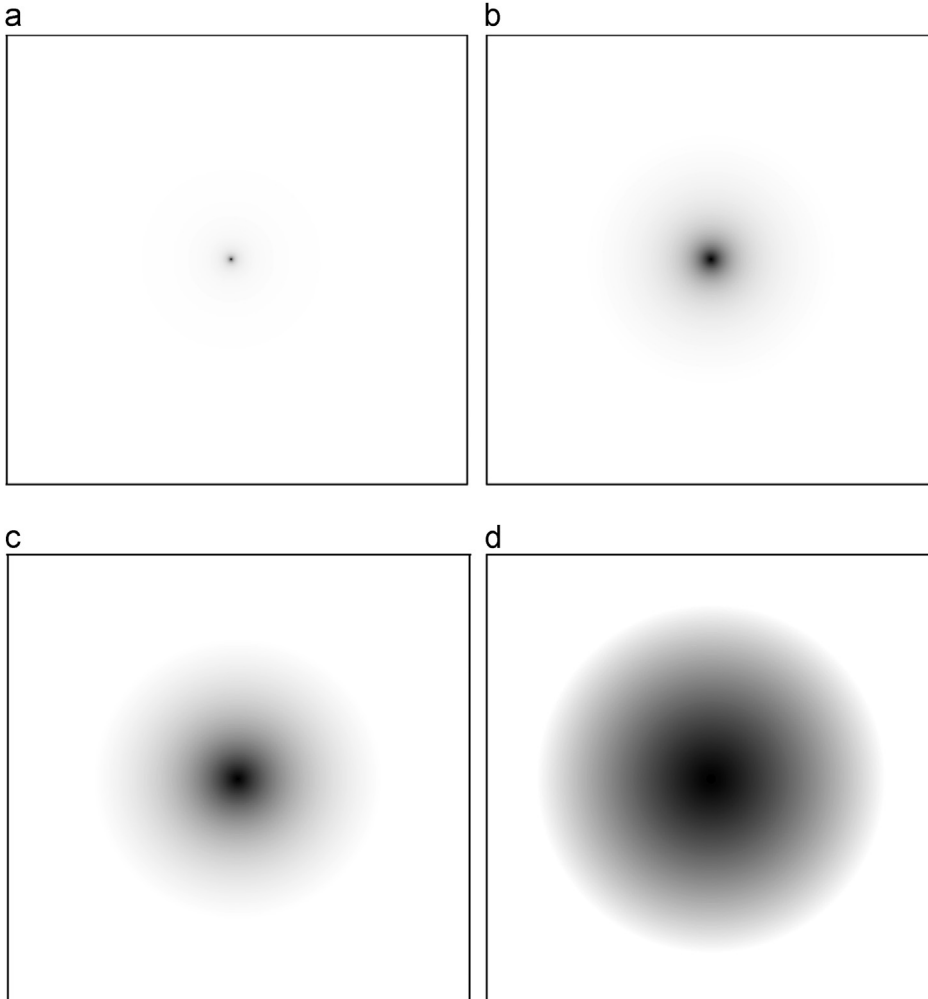


Fig. 2. Fourier spectrum of the PSI filter for (a) $t=1$, (b) $t=0.1$, (c) $t=0.03$, (d) $t=0.001$.

texture. As t changes so does the texture granularity (notice the log scale).

Fig. 2 shows the Fourier spectrum of the PSI filter. Notice that as t decreases, the radius from the center of non-preserved frequencies increases.

To see this more clearly, Fig. 3 depicts a transversal section of the PSI filter in the Fourier domain for different values of t . Here, we appreciate in detail the described behavior. As the value of t decreases passing frequencies

will diminish. Furthermore we can observe that the passing high frequency will be amplified. Notice that for values of $t < 10^{-3}$, the shape of the PSI filter almost does not vary, and therefore we can define the range of useful values of t in the interval $[10^{-3}, 1]$. In [13] it was found that the useful range of values was in the interval $(0, 1]$. Note, however, that in [13] the filter was not normalized so that its squared components add to 1, and, hence, t produces large variations that had to be compensated with large

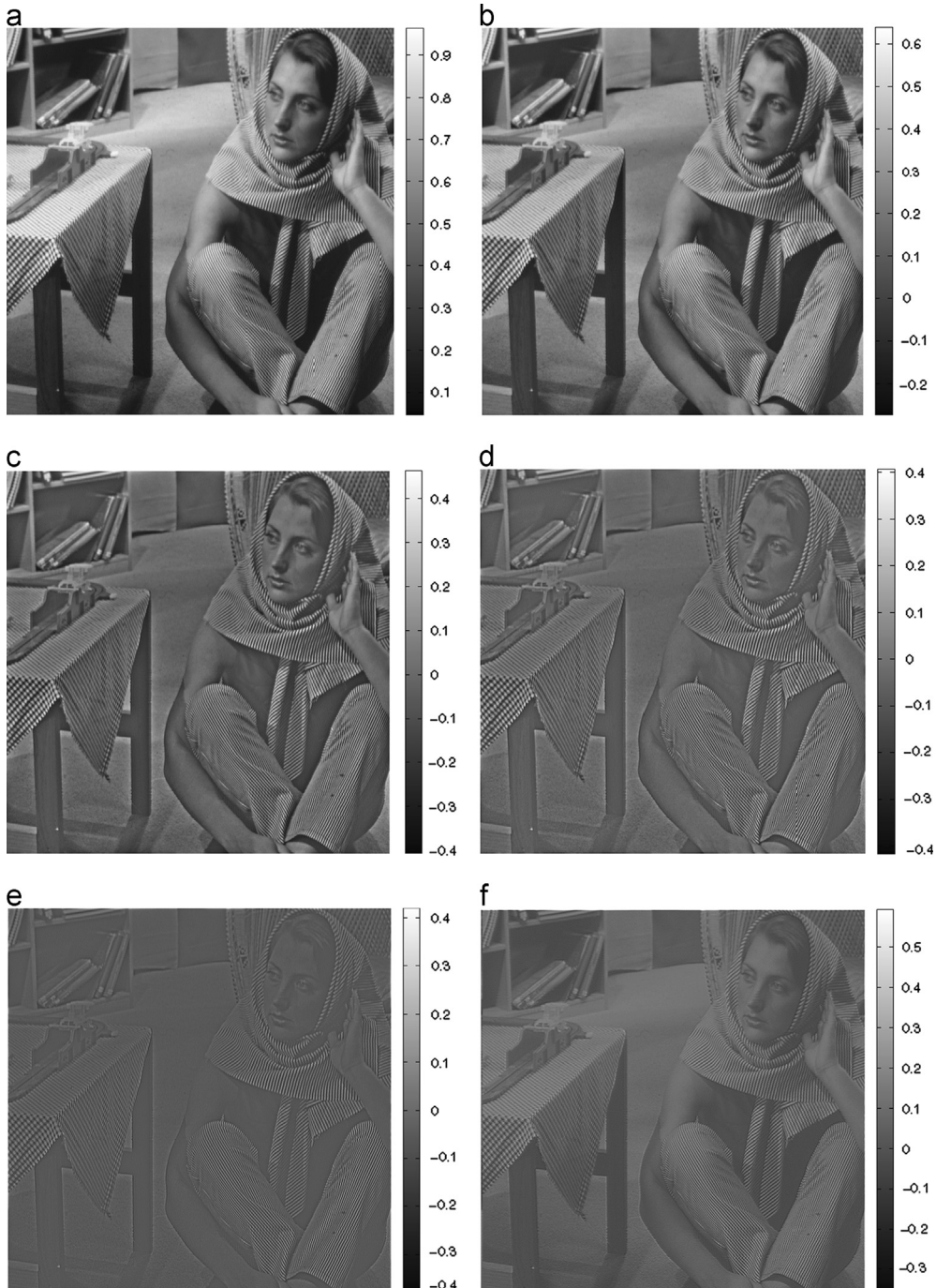


Fig. 4. (a) Original *Barbara* image, filtered images with (b) $t=1$, (c) $t=0.1$, (d) $t=0.03$, (e) $t=0.001$ and (f) SAR.

variations on the regularization parameter. For comparison purposes, Fig. 3 also shows a transversal section of the SAR filter. The SAR filter presents a frequency response similar to the PSI when the value of t is close to 0, specially in the middle frequencies, but it attenuates more the low frequencies and does not amplify very high frequencies.

As it is well known, the high frequencies in an image are associated with abrupt changes, fine details, edges, and unfortunately also to noise in the spatial domain. In Fig. 4(b) the original *Barbara* image in Fig. 4(a) was filtered using the PSI filter with a value of $t=1$, which produces an image very similar to the original where only a narrow band of low frequencies is eliminated. In Fig. 4(c, d) the filtered images with a parameter $t=0.1$ and $t=0.03$, respectively, are presented. In these figures the eliminated frequencies become more evident, smooth areas are lost, and the edges and fine details become sharper since the high frequencies are amplified. This effect is more notorious in Fig. 4(e) where the image was filtered using a value of $t=0.001$, and all but the textures are removed, and edges and fine details like the trousers, scarf and tablecloth are highlighted. Hence, as the value of t decreases, only high frequencies will be preserved and smooth regions will be removed. For comparison, Fig. 4(f) also shows the application of the SAR filter to the same image.

In this section, we have presented two prior models: the TV prior that preserves the edges but smooths textures and the PSI model that preserves the textures. To take advantage of the characteristics of both models, we combine them and define the following new prior:

$$p(\mathbf{x}|\alpha_1, \alpha_2) \propto \exp\left(-\alpha_1 \text{TV}(\mathbf{x}) - \frac{\alpha_2}{2} \|\mathbf{Z}\mathbf{x}\|^2\right). \quad (14)$$

Once the prior and degradation models are defined, we perform inference to estimate the original image.

3. Bayesian inference

In the inference stage we use the observation and prior models presented in the previous section to obtain a maximum *a posteriori* (MAP) estimation of the restored image.

The MAP, $\hat{\mathbf{x}}$, satisfies

$$\hat{\mathbf{x}} = \arg \min_{\mathbf{x}} \left\{ \frac{\beta}{2} \|\mathbf{y} - \mathbf{H}\mathbf{x}\|^2 + \alpha_1 \text{TV}(\mathbf{x}) + \frac{\alpha_2}{2} \|\mathbf{Z}\mathbf{x}\|^2 \right\}. \quad (15)$$

Finding $\hat{\mathbf{x}}$ is not an easy task due to the presence of the TV prior. However, by using Majorization–Minimization (MM) methods the MAP solution can be found iteratively [25]. Based on the average inequality [9], we utilize the following upper bound of the TV function:

$$\text{TV}(\mathbf{x}) \leq \frac{1}{2} \sum_{i=1}^P \frac{\Delta_i^h(\mathbf{x})^2 + \Delta_i^v(\mathbf{x})^2 + u_i}{\sqrt{u_i}} = \frac{1}{2} \mathbf{M}(\mathbf{x}, \mathbf{u}), \quad (16)$$

where $\mathbf{u} \in (\mathbb{R}^+)^P$ is a P -dimensional vector with components u_1, u_2, \dots, u_P that needs to be computed along with the image and has, as will be shown later, an intuitive interpretation related to the unknown image \mathbf{x} .

We then minimize

$$\bar{\mathcal{L}}(\mathbf{x}, \mathbf{u}) = \frac{\beta}{2} \|\mathbf{y} - \mathbf{H}\mathbf{x}\|^2 + \frac{\alpha_1}{2} \mathbf{M}(\mathbf{x}, \mathbf{u}) + \frac{\alpha_2}{2} \|\mathbf{Z}\mathbf{x}\|^2. \quad (17)$$

By alternating between the minimization of \mathbf{x} and \mathbf{u} .

For a given \mathbf{x} , we calculate \mathbf{u} as

$$\mathbf{u} = \arg \min_{\mathbf{u}} \sum_{i=1}^P \frac{\Delta_i^h(\mathbf{x})^2 + \Delta_i^v(\mathbf{x})^2 + u_i}{\sqrt{u_i}} \quad (18)$$

and, obtain

$$u_i = \Delta_i^h(\mathbf{x})^2 + \Delta_i^v(\mathbf{x})^2. \quad (19)$$

Note that vector \mathbf{u} is a function of the spatial first order differences of the unknown image \mathbf{x} and represents its local spatial activity.

For a given \mathbf{u} , to obtain the estimation of the image, first notice that Eq. (17) can be rewritten as

$$\bar{\mathcal{L}}(\mathbf{x}, \mathbf{u}) = \lambda \|\mathbf{y} - \mathbf{H}\mathbf{x}\|^2 + \lambda_1 \mathbf{M}(\mathbf{x}, \mathbf{u}) + \lambda_2 \|\mathbf{Z}\mathbf{x}\|^2, \quad (20)$$

with $\lambda = (1 - \lambda_1 - \lambda_2)$,

$$\lambda_1 = \frac{\alpha_1}{\beta + \alpha_1 + \alpha_2} \quad \text{and} \quad \lambda_2 = \frac{\alpha_2}{\beta + \alpha_1 + \alpha_2} \quad (21)$$

take values in the interval $[0, 1)$ and satisfy $\lambda + \lambda_1 + \lambda_2 = 1$. Thus, λ, λ_1 and λ_2 represent the relative influence on the restored image of the fidelity to the observed data and the combination of priors. Notice that selecting λ_1 and λ_2 in Eq. (20) is easier and more intuitive than selecting β, α_1 and α_2 in Eq. (17).

Then the MAP estimator, $\hat{\mathbf{x}}$, is obtained as the solution, utilizing for instance a conjugate gradient method, of the linear equation system

$$\mathbf{A}\mathbf{x} = \lambda \mathbf{H}^T \mathbf{y}, \quad (22)$$

where

$$\mathbf{A} = \lambda \mathbf{H}^T \mathbf{H} + \lambda_1 ((\Delta^h)^T \mathbf{W} \Delta^h + (\Delta^v)^T \mathbf{W} \Delta^v) + \lambda_2 \mathbf{Z}^T \mathbf{Z}, \quad (23)$$

Δ^h and Δ^v are the convolution matrices associated with horizontal and vertical gradients, respectively, and $\mathbf{W} = \text{diag}(1/\sqrt{u_i})$. This matrix controls the smoothness applied at each pixel of the image. So, for pixels in areas with a low spatial activity, the value of \mathbf{W} will be large, thus enforcing smoothness. In those areas, the PSI will be responsible for the texture preservation. However, for pixels in high spatial activity areas \mathbf{W} will be very small which means that no smoothness is enforced, thus preserving the edges and other features of the image.

The proposed restoration method is summarized in Algorithm 1.

Algorithm 1. Proposed restoration algorithm.

Require: An initial estimate of the original image, \mathbf{x}^0
 Set $k=0$
repeat
 1. Set $\mathbf{u}^k = \arg \min_{\mathbf{u}} \bar{\mathcal{L}}(\mathbf{x}^k, \mathbf{u})$.
 2. Set $\mathbf{x}^{k+1} = \arg \min_{\mathbf{x}} \bar{\mathcal{L}}(\mathbf{x}, \mathbf{u}^k)$.
 3. Set $k = k + 1$.
until $\|\mathbf{x}^{k+1} - \mathbf{x}^k\|^2 / \|\mathbf{x}^k\|^2 < \text{tol}$

Notice that if we fix λ_2 to zero in Eq. (23) we have a Bayesian formulation of the TV model and, when $\lambda_1 = 0$ we use only the PSI model.

4. Experimental results

Before comparing the proposed method with other restoration approaches, we assess the influence of the

parameter t . We blurred the region of the original *Barbara* image depicted in Fig. 5(a) scaled to the range $[0, 1]$, using a Gaussian kernel of size 21×21 and standard deviation 1, and then added white Gaussian noise of variance 10^{-3} .

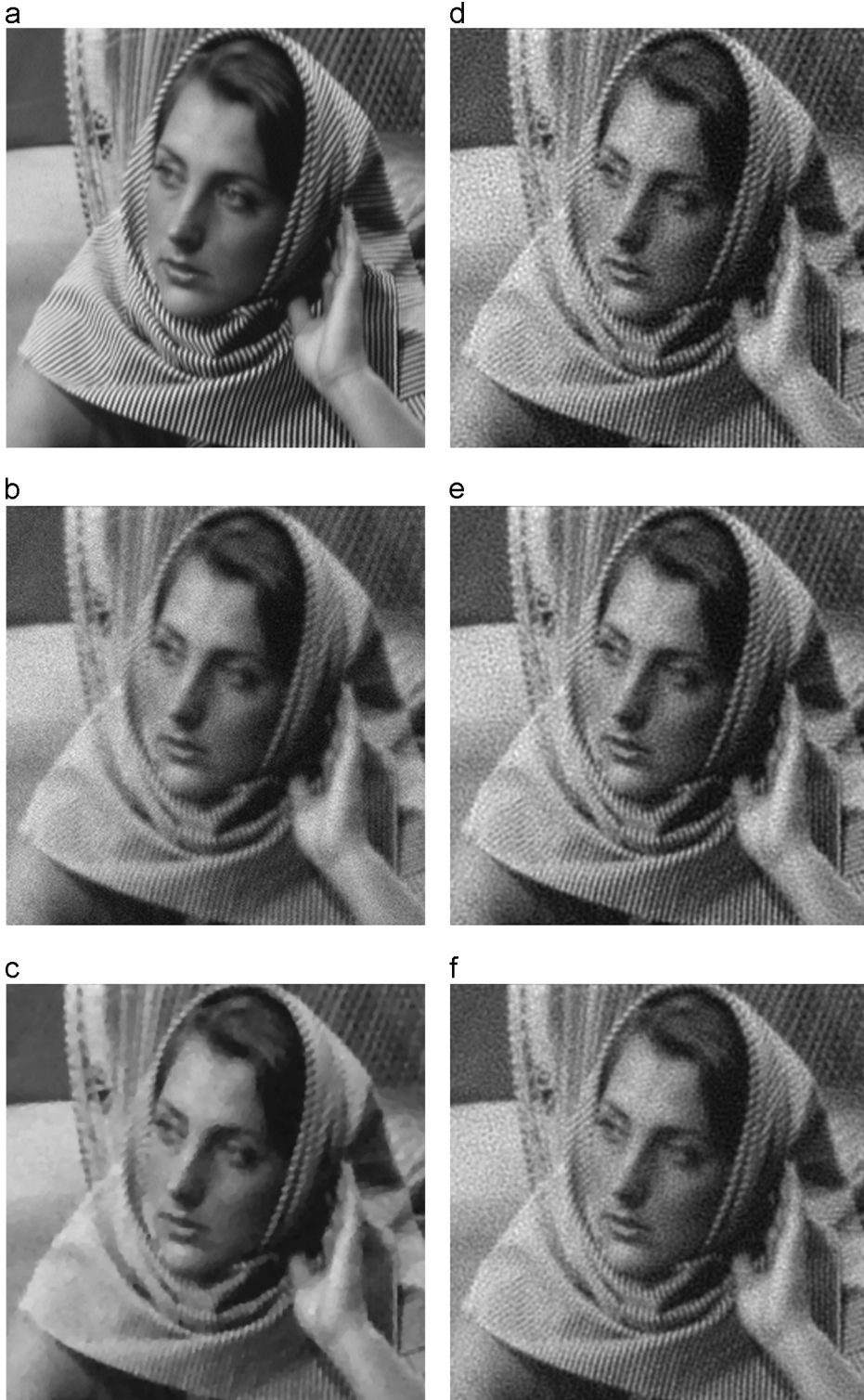


Fig. 5. (a) Original *Barbara* image, (b) degraded observation, (c) restoration with the TV model. Restorations with PSI method for (d) $t=0.001$, (e) $t=0.01$ and (f) $t=1$.

It produced the observation shown in Fig. 5(b), whose peak signal-to-noise ratio is PSNR=24.68 dB.

Since we want to assess the influence of t on the final restorations, we fixed $\lambda_1 = 0$, to see how the PSI restoration method works alone. Then we obtained the restoration for $\lambda_2 \in \{0, 10^{-7}, 10^{-6}, 10^{-5}, 10^{-4}, 10^{-3}, 10^{-2}, 0.1, 0.2, 0.3, 0.4\}$ and $t \in \{0.001, 0.01, 0.03, 0.1, 1\}$.

In Fig. 6(a), we plot the PSNR evolution for all considered couples of values (λ_2, t) . For a small value of λ_2 the PSI model has not much influence on the restorations that it is not enough regularized and then low PSNR values are obtained. When λ_2 increases, such influence is higher and the obtained restorations achieve up to appoint better PSNR values.

The maximum is reached at the point $(\lambda_2, t) = (0.1, 0.01)$, and for values of λ_2 higher than 0.1 the PSNR slightly decreases. Fig. 6(b) shows the PSNR values for fixed $\lambda_2 = 0.1$ and the different values of t , which highlights the influence of t on the final restorations.

To visually observe this behavior, Fig. 5(d)–(f) depicts the obtained restorations for $\lambda_2 = 0.1$ and $t = 0.001$, $t = 0.01$ and $t = 1$. When $t = 0.001$ we obtain the noisiest restoration

(Fig. 5(d)), but if we look at the scarf and the chair behind *Barbara* we can see that the textures are more pronounced than in the other two restorations. On the other extreme, when $t = 1$ (Fig. 5(f)) we obtain the smoothest and less noisy restoration, but textures are less marked. Finally, when $t = 0.01$ the restored image (Fig. 5(e)) has an acceptable level of noise, while the textures remain quite marked. Hence, there exists a trade-off between the restored textures and level of noise in the image, which can be tuned by modifying the value of the parameter t . As we mentioned before, this result is also numerically supported, since the PSNR values for the restoration of the image in Fig. 5(b) with $t = 0.001$ and $t = 1$ are 26.02 dB and 25.65 dB, respectively, while the best PSNR, 26.05 dB, is obtained for $t = 0.01$. For comparison purposes, we included in Fig. 5(c) the restoration with the TV model, obtained with Alg. 1 by setting $\lambda_1 = 0.01$ and $\lambda_2 = 0$, which has a PSNR of 25.02 dB. This is an almost noise free image but the textures in some parts of the scarf are lost.

From this experiment we can conclude that (a) neither the TV nor the PSI image models alone are able to successfully recover the textures and control the noise and (b) the parameter t of the PSI model will control the amount of texture in the image. In the following experiments we will show that a sensible combination of the TV and PSI models produces better results than using just one model alone.

To obtain the restored images using the TV, PSI, and TV+PSI priors, we run Alg. 1 starting from the degraded image as initial estimate of the original image, that is, $\mathbf{x}^0 = \mathbf{y}$, and used $tol = 10^{-4}$ for the stopping criterion in Alg. 1. To select the value of the parameters governing the weight of the TV and PSI prior models on the final restoration, λ_1 and λ_2 , we performed a search in the set of values $\{0, 10^{-7}, 10^{-6}, 10^{-5}, 10^{-4}, 10^{-3}, 10^{-2}, 0.1, 0.2, 0.3, 0.4\}$ and, as we have already indicated, we calculated the weight of the fidelity to the data term, λ , as $1 - \lambda_1 - \lambda_2$. Note that if $\lambda_2 = 0$, the TV model is used alone and that for $\lambda_1 = 0$ the PSI model is selected. We have experimentally observed that values of λ_1 or λ_2 larger than 0.4 reduce drastically the quality of the restored image so we did not consider them in our reported experiments. Additionally, the PSI prior in Eq. (13) depends on the parameter t . As we explained in Section 2.2, the range of useful values for this parameter is $\{10^{-3}, 1\}$ so, we explored the range $t \in \{0.001, 0.01, 0.03, 0.1, 1\}$.

We compared the performance of the proposed method with several classical and state-of-the art methods. First, we used the classical method in [12] that uses a simultaneous autoregressive (SAR) prior model obtains a MAP estimate of the image and, simultaneously, estimates the model parameters by maximum likelihood. Also, we compared with the method in [22] that proposes a combination of ℓ_1 and SAR prior models. The ℓ_1 prior model is similar to the TV prior but considers a different parameter for the horizontal and vertical first order differences. Following [22], we assumed an exact knowledge of the noise variance and let the method estimate only the ℓ_1 and SAR prior parameters. The combination parameter that controls the relative importance of the ℓ_1 and SAR restoration methods is selected by exploring the interval $[0, 1]$ in steps of 0.1 and selecting the one resulting in a better PSNR. The proposed

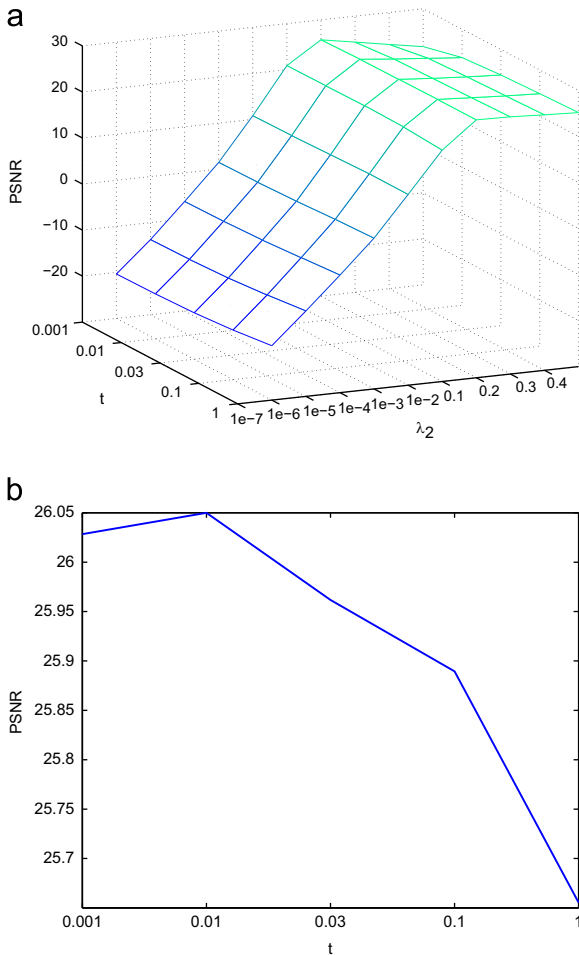


Fig. 6. (a) PSNR values for the restorations using the PSI model varying parameters λ_2 and t . (b) PSNR values for the restorations using the PSI model fixing $\lambda_2 = 0.1$ and varying parameter t .

method was also compared with the method in [13] which combines ℓ_2 and PSI prior models. The objective function in [13] to be minimized to estimate the original image has

the form

$$\mathcal{L}(\mathbf{x}) = \lambda^* \|\mathbf{y} - \mathbf{H}\mathbf{x}\|^2 + \lambda_1^* \|\mathbf{x}\|^2 + \lambda_2^* \|\mathbf{Z}\mathbf{x}\|^2,$$

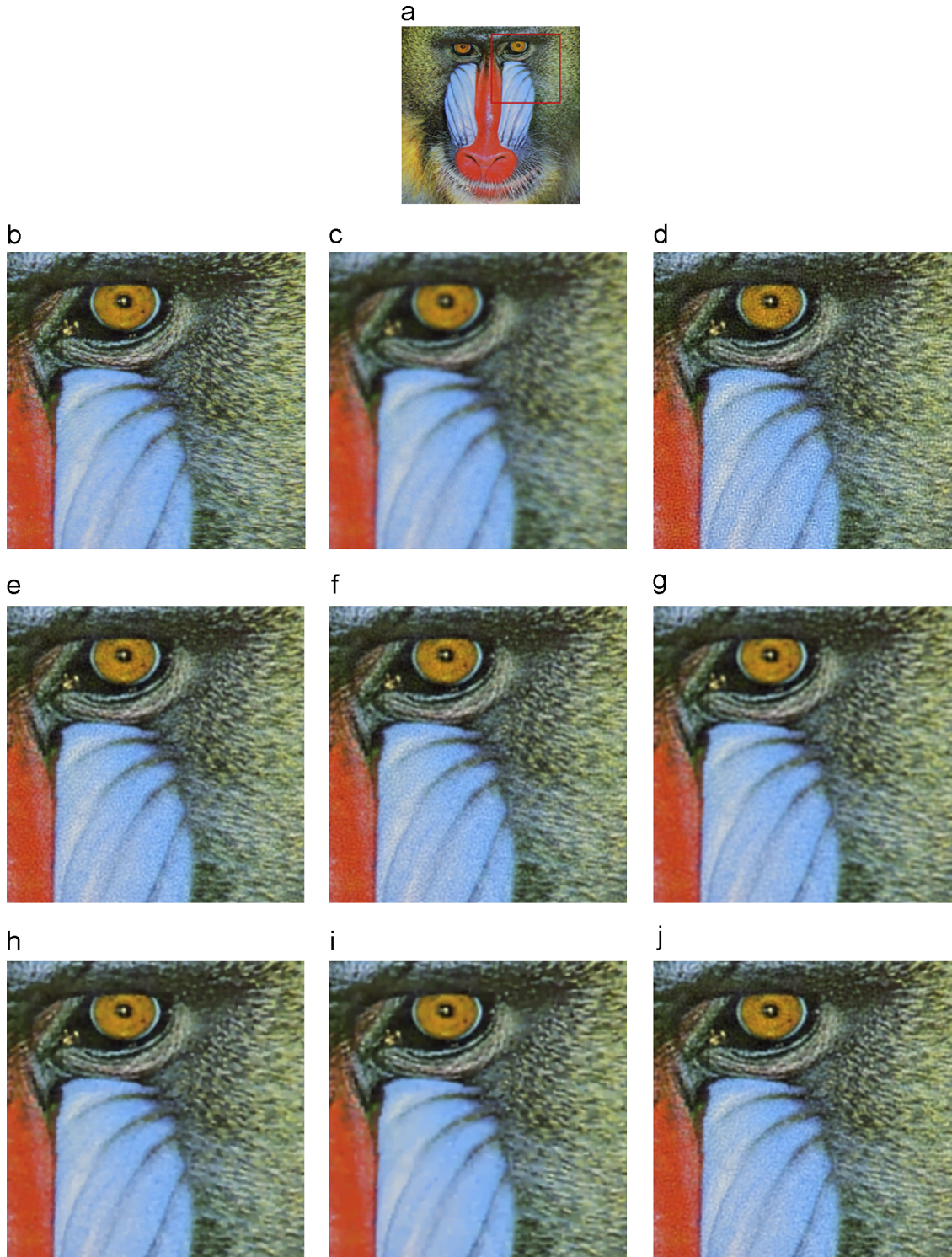


Fig. 7. (a) Original image with the area of interest marked, (b) area of interest of the original image, (c) degraded image, (d) restored image with the SAR model, (e) restored image with the PSI model, (f) restored image with the ℓ_2 +PSI model, (g) restored image with the ℓ_1 +SAR model, (h) restored image with the TV model, (i) restored image with the GSP model, (j) restored image with the proposed model.

with $\lambda^* = 1 - \lambda_1^* - \lambda_2^*$. We obtained restorations for $\lambda_1^*, \lambda_2^* \in \{0, 10^{-7}, 10^{-6}, 10^{-5}, 10^{-4}, 10^{-3}, 10^{-2}, 0.1, 0.2, 0.3, 0.4\}$ and $t \in \{0.001, 0.01, 0.03, 0.1, 1\}$ and reported the best results.

Finally, we compared with the recently proposed log model in [20], named *General Sparse Prior* (GSP). We want to note that, although the method in [20] was originally formulated



Fig. 8. (a) Original image with the area of interest marked, (b) area of interest of the original image, (c) degraded image, (d) restored image with the SAR model, (e) restored image with the PSI model, (f) restored image with the ℓ_2 +PSI model, (g) restored image with the ℓ_1 +SAR model, (h) restored image with the TV model, (i) restored image with the GSP model, (j) restored image with the proposed model.

as a blind deconvolution method, in this paper, we assume that the blur is known. We supplied the method with the real value for the noise variance.

We run all the restoration methods on four classic images in image processing: *Barbara*, *Cameraman*, *Baboon* and *Lena*. These test images have different levels of spatial activity and areas with different types of texture. The original images were synthetically degraded following the observation model in Eq. (1) after been scaled to the interval [0, 1]. Each image was blurred with a Gaussian blur with support 21×21 and standard deviation 1. Zero mean Gaussian noise with variance $\sigma_1^2 = 10^{-5}$, $\sigma_2^2 = 10^{-4}$ and $\sigma_3^2 = 10^{-3}$ was added to the blurred images to obtain three set of degraded images with SNR of about 50 dB, 40 dB and 30 dB, respectively. We repeated each experiment three times to decrease the dependence on a given realization of the noise and report the mean value of the results for all experiments.

We present detailed results on two representative images and noise combinations and, finally, we summarized and extract conclusions for the complete set of experiments.

Fig. 7(a) shows to the original *Baboon* image. To better appreciate the details in the images we show results in a small region of interest, marked with a square, of size 200×200 . In Fig. 7(b) the region of interest of the original image is depicted. It contains different features that allow us to evaluate how the method works. We can distinguish high frequency information as the hair or the details around the eye, as well as smoother zones as the nose. In Fig. 7(c) we shown the degraded image for a noise variance $\sigma_2^2 = 10^{-4}$. The PSNR for the whole image is 22.99 dB. Using the SAR model restoration is depicted in Fig. 7(d). Notice that this model restores the details in the

image; however, it also amplifies the noise, as can be seen in the nose. In fact, the PSNR for this restoration is smaller than the one of the observation, 22.85 dB. On the other side, TV and GSP models, whose restoration are shown in Fig. 7(h) and (i), respectively, obtain the smoothest restorations and similar PSNR values (24.54 dB for the TV model and 24.52 dB for the GSP model). The zone of the nose is almost noise-free, but the details around the eye and in the hair are smoothed out. The PSI, $\ell_2 + \text{PSI}$, $\ell_1 + \text{SAR}$ and the proposed method, shown in Fig. 7(e), (f), (g) and (j), respectively, achieve a good balance between noise and texture; however, if we compare the zone of the nose, we observe that the proposed method better eliminates the noise, while preserving a similar quality in textures. The numerical results also support this fact. PSI model alone obtains PSNR=24.71 dB, $\ell_2 + \text{PSI}$ model obtains PSNR=24.74, and the $\ell_1 + \text{SAR}$ gets PSNR=24.27 dB, while the proposed method obtains PSNR=24.86 dB.

For the image of *Barbara*, shown in Fig. 8(a), the same behavior is repeated. In this case, we have selected an area of interest of size 256×256 , which is marked by the square, and in Fig. 8(b). The degraded image was generated with noise variance $\sigma_2^2 = 10^{-4}$, Fig. 8(c), has PSNR=25.32 dB. In this case, the noise amplification and edge smoothness produced by the SAR model is much more evident (see Fig. 8(d)), getting PSNR=24.14 dB. The TV and GSP models in Fig. 8(h) and (i) manage to eliminate the noise almost completely, obtaining PSNR=26.75 dB and PSNR=26.73 dB, respectively. However, it can be appreciated that some textures in the scarf are lost. The PSI model (Fig. 8(e)), $\ell_2 + \text{PSI}$ model (Fig. 8(f)), $\ell_1 + \text{SAR}$ model (Fig. 8(g)) and TV+PSI model (Fig. 8(j)) are capable to restore the texture in the scarf and obtain PSNR=27.26 dB, PSNR=27.32, PSNR=25.93 dB and PSNR=27.55 dB, respectively. If we

Table 1
Peak signal to noise ratio results for *Baboon* and *Barbara* with different levels of noise.

Image	Method	PSNR (SNR=30 dB)	PSNR (SNR=40 dB)	PSNR (SNR=50 dB)
<i>Baboon</i>	Observation	22.27	22.99	23.06
	SAR	14.77	22.85	26.28
	PSI	23.10	24.71	26.06
	$\ell_2 + \text{PSI}$	23.10	24.74	26.28
	$\ell_1 + \text{SAR}$	22.62	24.27	25.74
	TV	22.65	24.54	26.19
	GSP	23.03	24.52	25.81
	TV + PSI	23.18	24.86	26.34
	Optimum parameters	$\lambda_1 = 10^{-3}$, $\lambda_2 = 10^{-1}$, $t=0.001$	$\lambda_1 = 10^{-4}$, $\lambda_2 = 10^{-2}$, $t=0.001$	$\lambda_1 = 10^{-5}$, $\lambda_2 = 10^{-3}$, $t=0.03$
	<i>Barbara</i>	Observation	24.16	25.32
SAR		14.45	24.14	30.74
PSI		24.87	27.26	29.91
$\ell_2 + \text{PSI}$		24.87	27.32	30.79
$\ell_1 + \text{SAR}$		24.54	25.93	29.29
TV		24.70	26.75	30.59
GSP		25.02	26.73	30.13
TV + PSI		24.93	27.55	30.93
Optimum parameters		$\lambda_1 = 10^{-3}$, $\lambda_2 = 10^{-1}$, $t=0.01$	$\lambda_1 = 10^{-4}$, $\lambda_2 = 10^{-2}$, $t=0.001$	$\lambda_1 = 10^{-5}$, $\lambda_2 = 10^{-3}$, $t=0.001$

Table 2
Peak signal to noise ratio results for *Lena* and *Cameraman* with different levels of noise.

Image	Method	PSNR (SNR=30 dB)	PSNR (SNR=40 dB)	PSNR (SNR=50 dB)
<i>Lena</i>	Observation	27.91	31.43	32.01
	SAR	15.09	24.67	33.33
	PSI	30.69	33.02	34.51
	ℓ_2 + PSI	30.69	33.02	34.58
	ℓ_1 + SAR	30.79	32.81	34.43
	TV	31.62	33.53	34.85
	GSP	31.52	32.94	33.45
	TV + PSI	31.62	33.61	34.91
	Optimum parameters	$\lambda_1 = 10^{-2}$, $\lambda_2 = 10^{-2}$, $t=0.001$	$\lambda_1 = 10^{-3}$, $\lambda_2 = 10^{-2}$, $t=0.001$	$\lambda_1 = 10^{-4}$, $\lambda_2 = 10^{-2}$, $t=0.001$
	<i>Cameraman</i>	Observation	24.51	25.82
SAR		14.38	24.15	30.67
PSI		25.95	27.85	30.38
ℓ_2 + PSI		25.95	28.24	30.55
ℓ_1 + SAR		25.71	28.02	30.13
TV		26.93	29.83	32.46
GSP		27.41	29.32	30.29
TV + PSI		26.94	29.84	32.47
Optimum parameters		$\lambda_1 = 10^{-2}$, $\lambda_2 = 10^{-6}$, $t=0.03$	$\lambda_1 = 10^{-3}$, $\lambda_2 = 10^{-5}$, $t=0.01$	$\lambda_1 = 10^{-4}$, $\lambda_2 = 10^{-5}$, $t=1$

look at top and left corner of the images, we can see that the proposed model again removes the noise better than the PSI, ℓ_2 +PSI and ℓ_1 +SAR models.

To summarize the experiments, in Tables 1 and 2 we report the mean PSNR values obtained in the experiments for the four images. We can see that the proposed method obtains the highest PSNR for all the restorations, except for the *Barbara* and *Cameraman* images when the noise variance is $\sigma_3^2 = 10^{-3}$. In these cases GSP obtains better results since it better controls high noise. Note that, in these cases, the differences between TV, GSP and TV+PSI methods are small for all the images. However, as the noise level is reduced the proposed TV+PSI method produces better results, especially in highly textured images. We want to note that the combination of PSI and TV models clearly improves over a single model, PSI or TV. In all the experiments the value of λ_1 and λ_2 was greater than zero, meaning that our method always included information from both models. Although we evaluated different values for the parameter t , it is worth mentioning that in most cases $t=0.001$ produces good results. Also the proposed method is competitive with the two state-of-the-art methods we compared with ℓ_1 +SAR model combination and GSP.

5. Conclusions

In this paper, we have presented a novel image restoration method that uses the Bayesian paradigm to combine two prior models: the TV model that preserves the edge structure while imposes smoothness on the solution and, the PSI model which is capable to preserve the textures. The final product is a restoration algorithm that combines the advantages of the two models. A study of PSI model and the parameter that controls its shape has been carried

out, and concluded that neither the TV nor the PSI image models alone successfully recover the textures and control the noise. Finally a set of experiments has been carried out, where the proposed method has been compared against both classical and state of art methods. The experimental results supported the proposed model and demonstrated that TV + PSI obtains high-quality restorations.

Future work will adapt the model to the local image characteristics and perform automatic parameter estimation within the Bayesian framework.

References

- [1] M. Elad, *Sparse and Redundant Representations*, Springer, 2010.
- [2] R. Molina, J. Núñez, F.J. Cortijo, J. Mateos, Image restoration in astronomy: a Bayesian perspective, *IEEE Signal Processing Magazine* 18 (2) (2001) 11–29.
- [3] A. Buades, B. Coll, J.M. Morel, A review of image denoising algorithms, with a new one, *Multiscale Model and Simulation* 4 (2005) 490–530.
- [4] K. Dabov, A. Foi, V. Katkovnik, K. Egiazarian, Image denoising by sparse 3-D transform-domain collaborative filtering, *IEEE Transactions on Image Processing* 16 (8) (2007) 2080–2095.
- [5] R. Yan, L. Shao, Y. Liu, Nonlocal hierarchical dictionary learning using wavelets for image denoising, *IEEE Transactions on Image Processing* 22 (12) (2013) 4689–4698. <http://dx.doi.org/10.1109/TIP.2013.2277813>.
- [6] L. Shao, R. Yan, X. Li, Y. Liu, From heuristic optimization to dictionary learning: a review and comprehensive comparison of image denoising algorithms, *IEEE Transactions on Cybernetics* PP (99) (2013) 1.1.0. <http://dx.doi.org/10.1109/TCYB.2013.2278548>.
- [7] L.I. Rudin, S. Osher, E. Fatemi, Nonlinear total variation based noise removal algorithms, *Physica D* (1992) 259–268.
- [8] S.D. Babacan, R. Molina, A.K. Katsaggelos, Parameter estimation in TV image restoration using variational distribution approximation, *IEEE Transactions on Image Processing* 17 (3) (2008) 326–339.
- [9] S.D. Babacan, R. Molina, A.K. Katsaggelos, Variational Bayesian blind deconvolution using a total variation prior, *IEEE Transactions on Image Processing* 18 (1) (2009) 12–26.
- [10] Z. Dogan, S. Lefkimiatis, A. Bourquard, M. Unser, A second-order extension of TV regularization for image deblurring, in: *Proceedings*

- of the 18th IEEE International Conference on Image Processing (ICIP), 2011, pp. 713–716.
- [11] F. Chen, X. Huang, W. Chen, Texture-preserving image deblurring, *IEEE Signal Processing Letters* 17 (12) (2010) 1018–1021.
 - [12] R. Molina, On the hierarchical Bayesian approach to image restoration. Applications to astronomical images, *IEEE Transactions on Pattern Analysis and Machine Intelligence* 16 (11) (1994) 1122–1128.
 - [13] A.S. Carasso, Singular integrals, image smoothness, and the recovery of texture in image deblurring, *SIAM Journal on Applied Mathematics* 64 (5) (2004) 1749–1774.
 - [14] L. Huang, L. Xiao, Z. Wei, Z. Zhang, Variational image restoration based on Poisson singular integral and curvelet-type decomposition space regularization, in: *Proceedings of the 18th IEEE International Conference on Image Processing (ICIP)*, 2011, pp. 685–688.
 - [15] J.-L. Stark, F. Murtagh, J.M. Fadili, *Sparse Image and Signal Processing*, Cambridge University, 2010.
 - [16] L. Wang, L. Xiao, J. Zhang, Z. Wei, New image restoration method associated with tetrolets shrinkage and weighted anisotropic total variation, *Signal Processing* 93 (4) (2013) 661–770.
 - [17] X. Shu, N. Ahuja, Hybrid compressive sampling via new total variation TVL1, in: *European Conference on Computer Vision (ECCV)*, 2010, pp. 393–404.
 - [18] J. Krommweh, J. Ma, Tetrolet shrinkage with anisotropic total variation minimization for image approximation, *Signal Processing* 90 (8) (2010) 2529–2539.
 - [19] S. Villena, M. Vega, D.S. Babacan, R. Molina, A.K. Katsaggelos, Bayesian combination of sparse and non-sparse priors in image super resolution, *Digital Signal Processing* 23 (2) (2013) 530–541.
 - [20] S.D. Babacan, R. Molina, M. Do, A.K. Katsaggelos, Blind deconvolution with general sparse image priors, in: *European Conference on Computer Vision (ECCV)*, 2012, pp. 341–355.
 - [21] E. Vera, M. Vega, R. Molina, A.K. Katsaggelos, Iterative image restoration using nonstationary priors, *Applied Optics* 52 (10) (2013) 102–110.
 - [22] M. Vega, J. Mateos, R. Molina, A.K. Katsaggelos, Astronomical image restoration using variational methods and model combination, *Statistical Methodology* 9 (1–2) (2012) 19–31.
 - [23] Y. Gousseau, J.-M. Morel, Are natural images of bounded variation? *SIAM Journal on Mathematical Analysis* (33) (2001) 634–648.
 - [24] M. Taibleson, On the theory of Lipschitz spaces of distributions on Euclidean n -space, *Journal of Mathematics and Mechanics* 13 (1964) 407–478.
 - [25] K. Lange, *Optimization*, Springer, 2004.